Hypersonic Viscous Static Stability of a Sharp 5-Deg Cone at Incidence

J.C. Adams Jr.* and B.J. Griffith†
ARO, Inc., Arnold Air Force Station, Tenn.

Static stability characteristics of a 5-deg semivertex angle sharp cone at angles of attack up to 4 deg are examined both theoretically and experimentally under hypersonic wind tunnel conditions. Interpretation of the experimental results is based upon a three-dimensional inviscid/laminar boundary-layer analysis and a three-dimensional hypersonic viscous shock layer analysis. It is shown that only the three-dimensional hypersonic viscous shock layer approach is capable of accurately predicting the static stability characteristics of a sharp cone at incidence under low Reynolds number hypersonic flow conditions where three-dimensional viscous interaction effects are dominant. Also considered are wall temperature effects on sharp cone at incidence static stability relative to extrapolation of hot-wall hypersonic wind tunnel results to cold-wall flight conditions.

Nomenclature

A_{base} = base surface area, $\pi D^2/4$
BL = boundary layer
C_A = axial-force coefficient, axial force/$q_\infty A_{base}$
$C_{f_{\infty,s}}$ = local streamwise skin-friction coefficient, τ_s/q_∞
$C_{f_{\infty,\phi}}$ = local circumferential skin-friction coefficient, τ_ϕ/q_∞
C_N = normal-force coefficient normal force/$q_\infty A_{base}$
C_M = pitching-moment coefficient about X_{cm}, pitching moment (about X_{cm})/$q_\infty A_{base} D$
C_{M_0} = pitching-moment coefficient about apex, pitching moment (about apex)/$q_\infty A_{base} L$
D = base diameter of cone
HVSL = hypersonic viscous shock layer
L = axial length of cone as defined in Fig. 1
M_∞ = freestream Mach number
p = local surface pressure on cone
p_{base} = cone base pressure
p_∞ = freestream static pressure
q_∞ = freestream dynamic pressure
Re_∞/ft = freestream unit Reynolds number
$Re_{\infty,L}$ = freestream Reynolds number based on axial length of cone
R/V = re-entry vehicle
s,n = surface-fixed coordinate system as defined in Fig. 1
T_{wall} = wall temperature
$T_{0,\infty}$ = freestream stagnation temperature
T_∞ = freestream static temperature
x = axial distance from cone apex as defined in Fig. 1
X_{cm} = axial center-of-moment location as defined in Fig. 1
X_{cp} = axial center-of-pressure location as defined by Eqs. (4) and (6)
α = angle of attack
γ = ratio of specific heats
δ_v = cone semivertex angle
τ_s = wall shear stress in s-direction
τ_ϕ = wall shear stress in ϕ-direction
ϕ = circumferential coordinate defined in Fig. 1

Sign Convention on C_M and C_{M_0}: A negative (−) sign on the pitching moment C_M or C_{M_0} denotes a nose-down moment relative to the nomenclature in Fig. 1.

Base Pressure Contribution to the Axial-Force Coefficient C_A: The base pressure is taken as equal to the freestream static pressure (i.e., $p_{base} = p_\infty$) in definition of the axial-force coefficient C_A.

Received May 27, 1975; revision received September 26, 1975. The research reported herein was conducted by the Arnold Engineering Development Center (AEDC), Air Force Systems Command (AFSC), U.S. Air Force. Research results were obtained by personnel of ARO, Inc., contract operator of AEDC. Further reproduction is authorized to satisfy needs of the U.S. Government.

Index categories: Supersonic and Hypersonic Flow; Entry Vehicle Dynamics and Control.

*Senior Scientist and Supervisor, Project Support and Special Studies Section, Aerodynamics Project Branch, von Karman Gas Dynamics Facility. Associate Fellow AIAA.

†Assistant Branch Manager, Aerodynamics Projects Branch, von Karman Gas Dynamics Facility. Associate Fellow AIAA.

Introduction

THE dramatic effects of boundary-layer transition moving up over the base of a slender hypersonic re-entry vehicle (R/V) relative to vehicle dynamics are well-documented in the literature.[1-3] Not nearly so well-known, however, are the hypersonic viscous effects on R/V static stability at incidence under low Reynolds number laminar flow conditions. Studies such as those of Penland[4,5] indicate that classical analysis techniques, for example, Newtonian theory,[6] are adequate for predicting the static stability characteristics of a sharp cone at incidence provided the flow is hypersonic and the boundary layer is laminar. The present paper reexamines this generally accepted belief among hypersonic aerodynamicists in view of recent hypersonic wind tunnel experiments and recently developed analysis tools for studying three-dimensional hypersonic viscous (laminar)

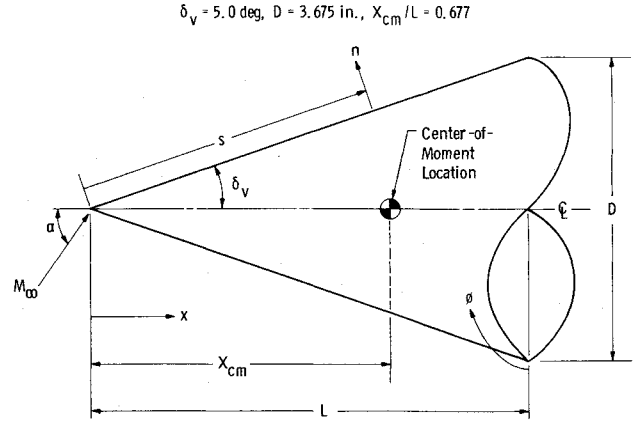

Fig. 1 Geometry and nomenclature for a sharp cone at angle of attack.

flowfields over slender conical R/V configurations at small to moderate angles of attack. Emphasis is placed upon delineation of hypersonic viscous effects on the static stability of a sharp cone at incidence under low Reynolds number laminar flow conditions. The approach is to apply existing documented analysis techniques for interpretation of AEDC von Karman Gas Dynamics Facility (VKF) Hypersonic Wind Tunnels (B) and (C) experiments using a specially designed balance to measure aerodynamic forces and moments on a 5.0° semivertex angle sharp cone at angles of attack up to 4° under low Reynolds number conditions.

Experimental Investigation

The experimental results reported in the present paper were obtained from an experimental program conducted in the AEDC-VKF Tunnels B (nominal Mach 8) and C(nominal Mach 10) designed to accurately measure force and moment characteristics of a 5.0° semivertex angle sharp cone at angles of attack up to 4° under laminar flow conditions. Details of the model geometry including pertinent nomenclature to be followed in the present paper are given in Fig. 1. Note that the model had a base diameter of 3.675 in. which resulted in a total model length of 21.0 in. The model itself was constructed of steel and fabricated with an interchangeable steel nose section, rear frustum, and base plate. A special water-cooled three-component force balance was designed and fabricated for use in this test program. The design criteria for this balance were as follows: 1) Normal-force loads up to 9 lbf ±5 gm, 2) Axial-force loads up to 1.5 lbf ± 1.5 gm, 3) Center-of-pressure location to 0.1% of model axial length.

The resultant balance performance generally met these design specifications. In addition, a slender sting arrangement was used which gave realistic base to freestream pressure ratios between 0.3 and 0.4 for all test conditions, thus providing mininal support interference of the sting on the resulting data. Overall repeatability of the aerodynamic data from run to run and tunnel entry to tunnel entry was ±0.0008 in normal-force coefficient C_N; ±0.0011 in pitching-moment coefficient C_M; ±0.0015 in axial-force coefficient C_A; and ±0.2% in center-of-pressure location based on model axial length. As a result of the balance sensitivity as well as the overall test requirements, nonstandard test procedures for hypersonic wind tunnel force measurements were employed. The AEDC-VKF model injection system was used to inject and remove the model from the test section while the tunnel was in operation. The obvious test requirement to record the maximum amount of useful information including repeat data in the shortest time interval after model injection dictated that a continuous angle-of-attack sweep mode of data recording be employed. This means that as the sector was manually pitched through an angle-of-attack range (at the rate of approximately 1°/sec), the test results were continuously recorded. Nominally, each measurement was recorded 50 times per sec. A single data point consisted of the average value of 14 recorded measurements on an individual input channel.

The experimental investigation was conducted under the following wind tunnel conditions which were specifically chosen to ensure laminar flow conditions over the entire model.

The model wall temperature to freestream stagnation temperature ratios are nominal values which are estimated to be accurate to within ±0.10. These fairly cool wall values reflect the injection of the model into the tunnel flow as discussed in the preceding.

Analytical Analysis

Three-Dimensional Inviscid Conical Flow

A recent investigation by Jones[7] resulted in an accurate and efficient numerical integration procedure for solution of the governing partial differential equations describing the supersonic or hypersonic inviscid perfect gas flowfield around a sharp cone at incidence. Basically, Jones method used the condition of conicity to reduce the problem to a set of elliptic nonlinear partial differential equations in two independent variables. A transformation of coordinates is used to fix the boundaries, one of which is the unknown shock wave, between which the elliptic equations are numerically solved using a relaxation procedure. The method is, in many cases, only limited by the crossflow velocity expanding from subsonic to supersonic conditions (which changes the mathematical character of the governing equations from elliptic to hyperbolic), by the entropy singularity moving too far away from the surface, or by the leeside shock approaching very close to the Mach wave. In practice these restrictions limit the maximum allowable angle of attack to a value on the order of or slightly greater than the cone semivertex angle.

It should be pointed out that Jones[8] has recently published a very complete and thorough set of tables for inviscid supersonic and hypersonic flow about sharp right circular cones at incidence in a perfect gas, $\gamma = 1.40$, stream. Included in these tables are tabulated axial- and normal-force coefficients over the freestream Mach number range from 1.5 to 20 for cone semivertex angles over the range of 5 to 40°.

Three-Dimensional Laminar Boundary-Layer (BL) Flow

The three-dimensional laminar boundary-layer analysis in the present investigation follows Appendix B of the report by McGowan and Davis.[9] The limiting forms of the full three-dimensional compressible laminar boundary-layer equations for conical flow are solved using a marching implicit finite-difference technique for numerical integration of the nonlinear parabolic partial differential equations written in similarity variable form. A thermally and calorically perfect air model is used having a constant specific heat ratio of $\gamma = 1.40$ in conjunction with the Sutherland viscosity law and a constant laminar Prandtl number of 0.71. All inviscid data necessary for input to the McGowan and Davis boundary-layer analysis (namely, the circumferential surface pressure distribution around the cone along with the inviscid surface velocity and density on the windward streamline) are taken from the Jones inviscid analysis described in the preceding. Illustrative examples of the application of the McGowan and Davis boundary-layer analysis for laminar flow over a sharp cone at incidence under hypersonic conditions are given in the report by Adams.[10] More recent work by Adams[11] extends the McGowan and Davis laminar analysis to include turbulent boundary-layer flow on sharp cones at incidence under both supersonic and hypersonic conditions.

Three-Dimensional Hypersonic Viscous Shock Layer (HVSL) Flow

The most applicable and accurate analytical technique currently available for the analysis of hypersonic flow over a sharp cone at incidence is the HVSL approach by Lubard and Helliwell.[12] An approximate system of governing equations is obtained from the complete steady-state compressible Navier-Stokes equations by assuming that the viscous, streamwise derivative terms are small compared with the viscous normal and circumferential derivatives. The resulting equations are valid in both the inviscid and viscous regions including the cir-

Table 1 Test conditions

Tunnel	M_∞	Re_∞/ft	$T_{0,\infty}$(°R)	T_∞(°R)	p_∞(lbf/ft^2)	$T_{wall}/T_{0,\infty}$
B	7.93	0.880×10^6	1300	94.0	2.802	0.55
C	9.96	1.030×10^6	1900	94.1	2.437	0.43

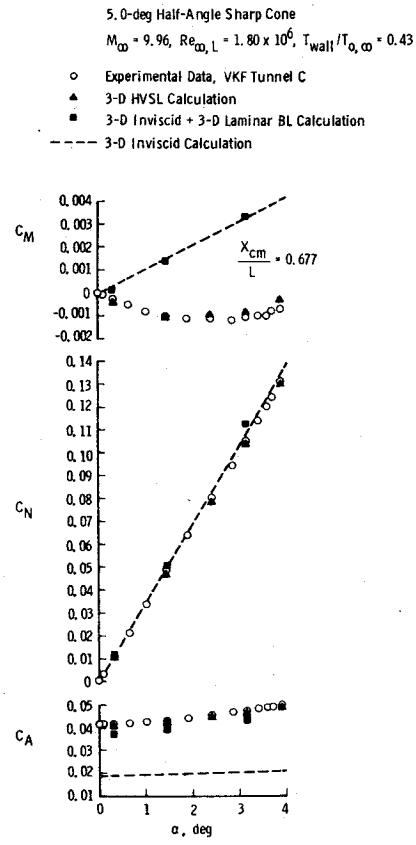

Fig. 2 Force and moment coefficients at Mach 10 VKF Tunnel C conditions.

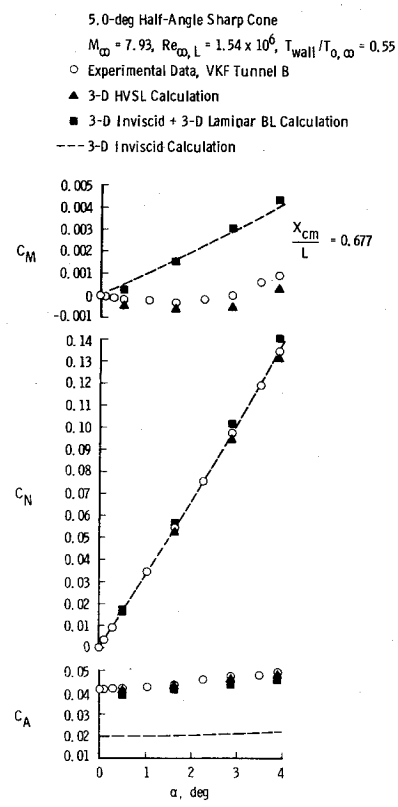

Fig. 3 Force and moment coefficients at Mach 8 VKF Tunnel B conditions.

cumferential separation zone which develops on the leeward side at the higher angles of attack (greater than approximately the cone semivertex angle). Since this set of governing partial differential equations is parabolic in the streamwise direction, a marching-type numerical solution technique is used. An implicit finite-difference treatment is applied to the normal derivatives in conjunction with Newton's method of iteration for solution of the nonlinear algebraic equations which result from differencing of the circumferential derivatives. The equations are solved between the body surface and the bow shock; boundary conditons at the shock and its resulting shape are calculated by using the Rankine-Hugoniot shock-crossing relations and a one-sided differencing of the continuity equation. A thermally and calorically perfect air model is used having a constant specific heat ratio of $\gamma = 1.40$ in conjunction with the Sutherland viscosity law and a constant laminar Prandtl number of 0.71. The digital computer code is discussed in the recent paper by Adams.[13]

It is important to note and appreciate that the HVSL approach includes both the inviscid and viscous regions of the flowfield in one composite set of equations. Hence complicated inviscid-viscous interactions which occur under hypersonic flow conditions (such as the well-known displacement-induced pressure effect) are automatically included in the analysis without tedious matching of separate inviscid and viscous solutions as would be required using higher order boundary-layer theory.

Computational Details

All numerical calculations reported in the present paper were performed on an IBM 370/165 digital computer using double precision arithmetic. Resulting numerical output from these analyses with respect to surface pressure and surface shear stress distributions were numerically integrated to yield the computed static stability coefficients presented in this paper. In the definition of the pressure contribution to the axial-force coefficient C_A the base pressure is taken to be equal to the freestream static pressure.

Results and Discussion

Force and Moment Coefficients

Presented in Figs. 2 and 3 are the experimentally determined force and moment coefficients relative to the various analysis techniques. The large viscous effects on the axial-force coefficient C_A are strikingly apparent. Note that the HVSL analysis is in excellent agreement with the C_A data over the entire angle-of-attack range, whereas the BL analysis consistently underpredicts the magnitude of C_A by some 6-8%. With respect to the normal-force coefficient C_N both the inviscid and HVSL analyses are in reasonable agreement with the data, whereas the BL analysis overpredicts the magnitude of C_N by some 4-6%. Results from Newtonian theory for a sharp cone at incidence,[6]

$$C_A = 2\sin^2\delta_v + (1 - 3\sin^2\delta_v)\sin^2\alpha \quad (1)$$

$$C_N = \cos^2\delta_v \sin 2\alpha \quad (2)$$

are in good agreement with the present inviscid calculations.

The situation is markedly changed upon examination of the pitching-moment coefficient C_M in Figs. 2 and 3. Both the inviscid and BL analyses predict the cone to be statically unstable relative to the center-of-moment location $X_{cm}/L = 0.677$. The experimental data and the HVSL analysis show that the cone will be marginally statically stable for small angles of attack but statically unstable at higher angles of attack. Thus, for the present moment-reference location, both the inviscid and laminar BL analyses fail to yield even the correct trend with respect to changes in pitching moment at varying angles of attack. The HVSL analysis, however, gives both the correct (nonlinear) trend and reasonably accurate estimates for the magnitude of C_M as angle of attack is

varied. Results from Newtonian theory for a sharp cone at incidence,[6]

$$C_M = \frac{\cos^2\delta_v \sin 2\alpha}{2\tan\delta_v}\left[\frac{X_{cm}}{L} - \frac{2}{3\cos^2\delta_v}\right] \quad (3)$$

are in excellent agreement with the present inviscid calculations; thus the comments relative to failure of an inviscid analysis apply equally well to Newtonian theory.

Center-of-Pressure Location

The so-called center-of-pressure location X_{cp}/L relative to the sharp cone apex as defined by the relationship

$$\frac{X_{cp}}{L} = \frac{X_{cm}}{L} - \frac{2C_M \tan\delta_v}{C_N} \quad (4)$$

is given in Fig. 4. It should be noted that C_M and C_N are the total or resultant pitching-moment and normal-force coefficients, respectively, and hence reflect both pressure and viscous forces and moments. For angles of attack greater than about one degree the HVSL analysis is in excellent agreement with the experimental measurements; the trend of rearward shift in X_{cp}/L with decreasing angle of attack is well-predicted by the HVSL analysis. Small differences between small numbers, i.e., numerical precision problems, explain the discrepancy between experiment and the HVSL analysis at small angles of attack (less than one degree) where the numerical values for both C_M and C_N are approaching zero. Because of the conical nature of the three-dimensional inviscid flowfield, the inviscid prediction of the X_{cp}/L location is identical to that derived from Newtonian theory,[6]

$$\frac{X_{cp}}{L} = \frac{2}{3\cos^2\delta_v} \quad (5)$$

as shown by Garcia.[14] Note from Fig. 4 that addition of laminar BL effects to the inviscid prediction has little effect on the predicted X_{cp}/L location. Only the HVSL analysis is applicable to determination of center-of-pressure locations and trends with respect to anlge-of-attack effects; a Newtonian analysis or an inviscid analysis coupled with a laminar boundary layer does not yield accurate estimates.

Component Analysis

It is now in order to specifically examine the various individual components which sum to yield the previously discussed force and moment coefficients in order to understand the differences in predictions between the HVSL analysis and the inviscid analysis coupled with the laminar BL analysis. Presented in Table 2 are the various calculated components (streamwise skin friction, circumferential skin friction, and pressure) which sum to yield the total coefficient (be it axial force, normal force, or pitching moment) for a 3.16° angle of attack under the Mach 9.96 AEDC-VKF Tunnel C conditions. With respect to axial-force coefficient C_A the major difference is in the pressure contribution; the streamwise skin-friction contributions are essentially identical between the two analyses. Note that the streamwise skin-friction contribution is essentially identical in magnitude to the pressure contribution, i.e., viscous skin-friction effects are equally as important as pressure effects for this slender cone.

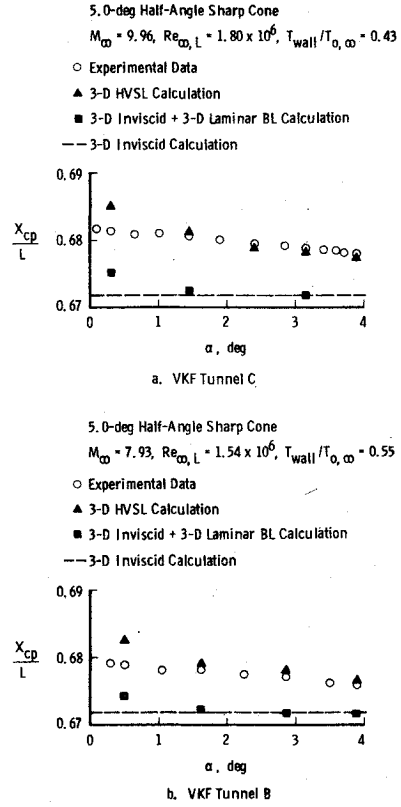

Fig. 4 Center-of-pressure variation with angle of attack.

Table 2 Sharp cone at incidence static stability characteristics; $\delta_v = 5.0°$, $\alpha = 3.16°$, $M_\infty = 9.96$, $Re_{\infty,L} = 1.80 \times 10^6$, $T_{wall}/T_{0,\infty} = 0.43$

		Components and resultant total			
	Type of analysis	Streamwise skin friction	Circumferential skin friction	Pressure ($p_{base} = p_\infty$)	Resultant total
C_A	3 – D HVSL	0.02343	0.0	0.02328	0.04671
	3 – D Inviscid + 3 – D Laminar BL	0.02321	0.0	0.02046	0.04367
C_N	3 – D HVSL	−0.00064	0.00467	0.09977	0.10380
	3 – D Inviscid + 3 – D Laminar BL	−0.00058	0.00537	0.10808	0.11287
C_{M_0}	3 – D HVSL	0.0	−0.00286	−0.06756	−0.07042
	3 – D Inviscid + 3 – D Laminar BL	0.0	−0.00322	−0.07261	−0.07583
$\frac{X_{cp}}{L}$	3 – D HVSL				0.67842
	3 – D Inviscid + 3 – D Laminar BL				0.67183

The pressure contribution to the normal-force coefficient C_N is again responsible for the major portion of the disagreement between analyses. The circumferential skin-friction contribution acts to slightly increase the normal force, as expected, whereas the streamwise skin-friction contribution results in a very small decrease in normal force. Similar comments apply with respect to the pitching-moment coefficient C_{M_0} (note from the Nomenclature that C_{M_0} is defined relative to the sharp cone apex with the distance L shown in Fig. 1 as the reference length). Again the pressure contribution is responsible for the major portion of the disagreement between analyses. The streamwise skin friction does not contribute to the pitching moment about the sharp cone apex because the streamwise skin friction acts through the sharp cone apex.

Center-of-pressure location X_{cp}/L relative to the sharp cone apex is determined from the relationship

$$\frac{X_{cp}}{L} = \frac{|C_{M_0}|}{C_N} \tag{6}$$

where C_{M_0} and C_N are the total or resultant pitching-moment and normal-force coefficients, respectively. Conversion between the pitching-moment coefficient C_M about the center-of-moment location X_{cm}/L as shown previously in Figs. 2 and 3, and the previously defined pitching-moment coefficient C_{M_0} about the sharp cone apex is given by the transfer relation

$$C_M = \frac{C_{M_0} + (X_{cm}/L)C_N}{2\tan\delta_v} = \frac{-C_N[(X_{cp}/L) - (X_{cm}/L)]}{2\tan\delta_v} \tag{7}$$

where the term in the denominator reflects that C_M uses the base diameter of the cone as the reference length. Note the C_M, C_{M_0}, and C_N are the total or resultant coefficients. From the preceding discussion concerning pressure effects on C_N and C_{M_0}, it may be concluded that these pressure effects are the cause of the rearward shift in center-of-pressure location as shown previously in Fig. 4.

The component analysis has indicated that the pressure component is the major source of disagreement between the HVSL approach and the inviscid analysis coupled with a laminar BL analysis relative to force and moment coefficients. As can be seen in Fig. 5, which gives the calculated streamwise surface pressure distributions at three circumferential locations ($\phi = 0$, 90, and 180°), the HVSL analysis yields a varying pressure along the cone as opposed to the constant pressure of the inviscid conical analysis. Figure 6 gives the circumferential pressure distribution at the body location $x/L = 0.677$ which reveals that, for this location, the windward ray ($\phi = 0°$) pressure from the HVSL is only 3% greater than the corresponding inviscid value, whereas on the leeward ray ($\phi = 180°$) the HVSL pressure is some 25% above the inviscid value. It is the combined effect of both the streamwise and circumferential pressure distribution variations given by the HVSL analysis as compared with the inviscid conical distribution (which is constant in value with respect to streamwise distance at a given circumferential location) that is responsible for the integrated pressure effects on the force and moment coefficients. The streamwise pressure variation in the HVSL analysis reflects the so-called viscous interaction which has an important (and in some cases dominant) effect on slender sharp cone drag at zero angle of attack under hypersonic conditions.[15,16] For slender sharp cones at incidence, the results of Refs. 17 and 18 clearly show the importance of viscous interaction because of the three-dimensional viscous interaction" treatment. Thus one may properly term the present HVSL approach a "three-dimensional viscous interaction" treatment.

A companion investigation of both the streamwise and circumferential skin-friction distributions is given in Figs. 7 and 8, respectively. As shown in Fig. 7, the calculated streamwise

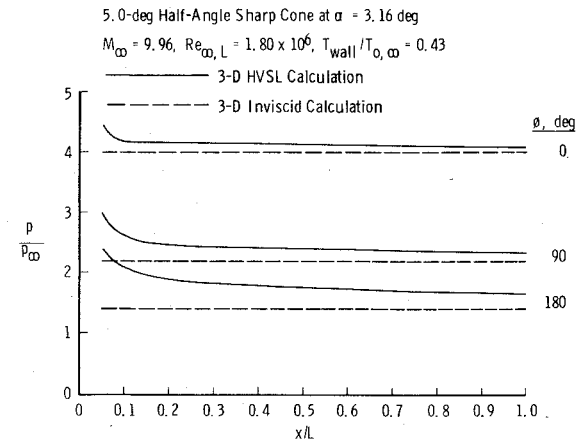

Fig. 5 Streamwise pressure distribution.

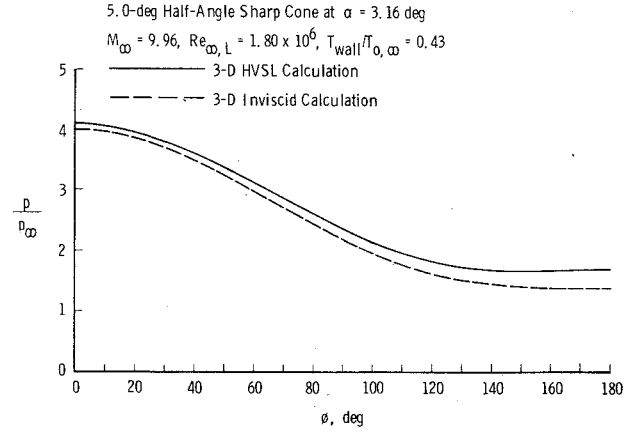

Fig. 6 Circumferential pressure distribution at body location $x/L = 0.677$.

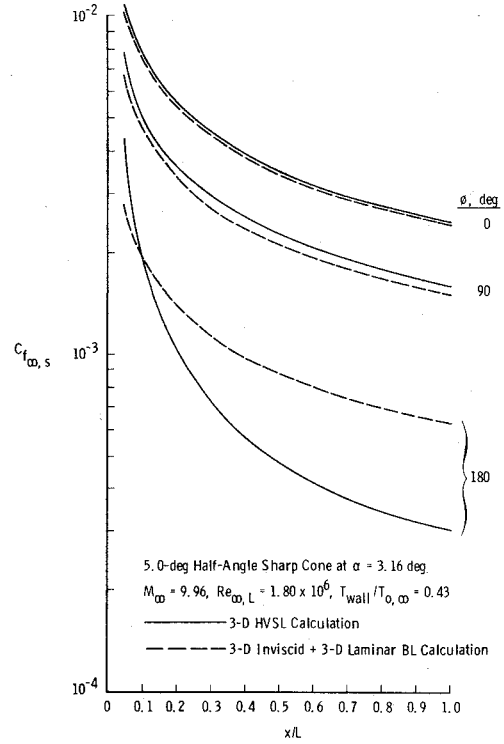

Fig. 7 Streamwise skin-friction distribution.

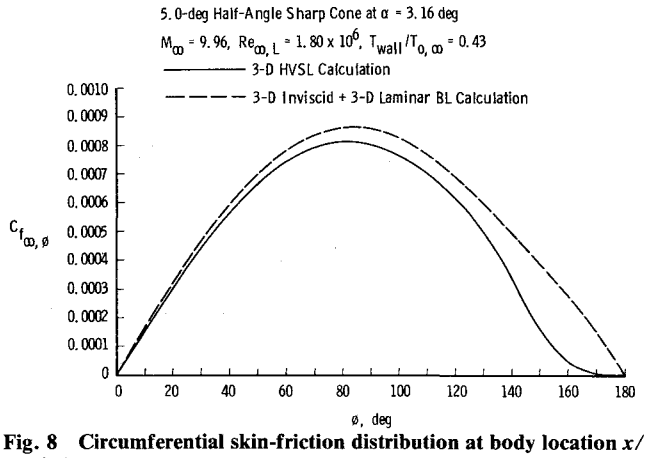

Fig. 8 Circumferential skin-friction distribution at body location $x/L = 0.677$.

skin-friction distribution from the laminar BL analysis is in good agreement with the HVSL analysis for the windward ($\phi = 0°$) and the ($\phi = 90°$) circumferential locations. Along the leeward ray ($\phi = 180°$) the streamwise distributions from the two analyses are quite different in both level and trend; this is due to the well-known failure of the three-dimensional boundary-layer equations at the leeward plane of symmetry.[19,20,21] Figure 8 shows that, for the body location $x/L \simeq 0.677$, the calculated circumferential skin-friction distributions from the HVSL and the laminar BL analyses are in reasonably good agreement up to approximately $\phi = 130°$ to 140°, where the upstream influence of the leeward ray ($\phi = 180°$) is reflected in the character of the HVSL distribution.

The important point from this discussion is that in regions where the magnitude of the streamwise and circumferential skin friction is large enough to influence integrated forces and moments, the laminar BL analysis and the HVSL analysis are in reasonably good agreement. It is the three-dimensional viscous interaction contribution to the streamwise and circumferential pressure distribution which is the important fluid mechanical effect accounted for by the HVSL analysis but neglected in the inviscid/laminar BL analysis. What may appear to be small increases in leeside pressure attributable to three-dimensional viscous interaction can result in substantial and even dominant effects on integrated forces and moments; the present pitching-moment results are an excellent example.

Wall Temperature Effects

Conventional hypersonic wind tunnel static stability tests are usually performed under what may be termed hot-wall conditions in that the model wall temperature is on the order of 70 to 80% of the freestream stagnation temperature. This is in contrast to atmospheric re-entry flight where the wall temperature of the R/V is on the order of 2 to 10% of the freestream stagnation temperature. Hence the important question is what is the effect of wall to stagnation temperature ratio on static stability parameters holding the freestream conditons and angle of attack fixed at given values. Presented in Table 3 for three wall to stagnation temperature ratios ($T_{wall}/T_{0,\infty} = 0.10$, 0.43, and 0.80) are the various calculated components (streamwise skin friction, circumferential skin friction, and pressure) which sum to yield the total coefficient (be it axial force, normal force, or pitching moment) for the same 3.16° angle of attack under Mach 9.96 AEDC-VKF Tunnel *C* conditions considered earlier with respect to Table 2. These calculated results are based upon the HVSL approach, which has been shown previously in this paper to be the most applicable and accurate analysis technique of those under current examination. The results shown in Table 3 reveal the following general trends.

1) Increasing wall temperature ratio increases both the streamwise skin friction and pressure contributions to the axial-force coefficient such that the resultant total axial-force coefficient is also increased.

2) Increasing wall temperature ratio increases the magnitude of both the streamwise and circumferential skin-friction contributions to the normal-force coefficient. However, increasing wall temperature ratio sufficiently decreases the pressure contribution to the normal-force coefficient such that the resultant total normal-force coefficient is decreased.

3) Increasing wall temperature ratio increases the circumferential skin-friction contribution to the pitching-moment coefficient. However, increasing wall temperature ratio sufficiently decreases the pressure contribution to the pitching-moment coefficient such that the resultant total pitching-moment coefficient is decreased.

4) Increasing wall temperature ratio increases the center-of-pressure location, i.e., an increasingly rearward shift in center-of-pressure location.

Examination of the individual components in Table 3 clearly shows that the wall temperature effect on the pressure contribution is the dominant cause for the previously discussed static stability coefficient behavior. This conclusion is reasonable in view of the well-known effects of increasing wall temperature on hypersonic laminar boundary-layer characteristics; the hotter the wall, the greater the effects of viscous interaction.

Conversion of the total or resultant pitching-moment coefficient C_{M_0} about the sharp cone apex from Table 3 using Eq.

Table 3 Wall temperature effects on sharp cone at incidence static stability characteristics based on 3-D HVSL analysis; $\delta_v = 5.0°$, $\alpha = 3.16°$, $M_\infty = 9.96$, $Re_{\infty,L} = 1.80 \times 10^6$

	T_{wall}	Components and resultant total			
		Streamwise skin friction	Circumferential skin friction	Pressure ($p_{base} = p_\infty$)	Resultant total
C_A	0.10	0.02253	0.0	0.02204	0.04457
	0.43	0.02343	0.0	0.02328	0.04671
	0.80	0.02338	0.0	0.02441	0.04779
C_N	0.10	−0.00059	0.00299	0.10398	0.10638
	0.43	−0.00064	0.00467	0.09977	0.10380
	0.80	−0.00065	0.00575	0.09429	0.09939
C_{M_0}	0.10	0.0	−0.00181	−0.07012	−0.07193
	0.43	0.0	−0.00286	−0.06756	−0.07042
	0.80	0.0	−0.00354	−0.06407	−0.06761
$\frac{X_{cp}}{L}$	0.10				0.67616
	0.43				0.67842
	0.80				0.68025

(7) yields the following results (Table 4) in terms of the pitching moment coefficient C_M about the center-of-moment location $X_{cm}/L=0.677$ as a function of wall temperature ratio:

Table 4 Wall temperature effects on pitching moment

$T_{wall}/T_{0,\infty}$	C_M
0.10	0.00051
0.43	−0.00084
0.80	−0.00185

For the present center-of-moment location, the cone will be statically stable for the hot-wall conditions but will become statically unstable under cold-wall conditions.

These results indicate that the hotter the wall, the greater the effects of three-dimensional viscous interaction on the static stability characteristics of a sharp cone at incidence under hypersonic conditions. The important point, however, is that hot-wall static stability data based on hypersonic wind tunnel tests must be suitably extrapolated to cold-wall flight conditions even if the freestream conditions (Mach number and Reynolds number) are reasonably well-matched. Further, simple Mach number/Reynolds number scaling between mismatched wind tunnel and flight conditions which, in turn, does not take into account wall temperature effects can result in erroneous conclusions regarding static stability characteristics of slender sharp cones at incidence.

Concluding Summary

The present paper has shown, by comparison with recently obtained hypersonic wind tunnel data, that classical aerodynamic analysis techniques (such as Newtonian or an appropriate three-dimensional inviscid theory coupled with a three-dimensional laminar boundary-layer analysis) are indeed applicable and reasonably accurate for determination of axial- and normal-force characteristics of a sharp slender cone at small to moderate angles of incidence under hypersonic low Reynolds number laminar flow conditions. However, the same classical analysis techniques fail to yield even the correct trend with respect to angle-of-attack effects on the static stability parameters of pitching moment and center-of-pressure location; only a full three-dimensional hypersonic viscous shock layer approach is applicable and accurate for determination of both the trend and magnitude of these parameters. The basic applicability of the three-dimensional hypersonic viscous shock layer approach is shown to be directly attributable to the fact that this type of analysis technique implicitly includes the effects of three-dimensional viscous interaction on the surface pressure distribution over a sharp cone at incidence. What may appear to be small local viscous interaction effects on both the streamwise and circ- sharp cone at incidence. What may appear to be small local viscous interaction effects on both the streamwise and circumferential surface pressure distributions can result in dominant, integrated effects with respect to static stability characteristics of a slender sharp cone at incidence under hypersonic low Reynolds number laminar flow conditions. These results clearly suggest that classical analysis techniques must be modified to properly include three-dimensional viscous interaction before they will become applicable and accurate for estimation of the static stability of a sharp cone at incidence in low Reynolds number hypersonic flow.

References

[1] Ericsson, L.E., "Effect of Boundary-Layer Transition on Vehicle Dynamics," *Journal of Spacecraft and Rockets*, Vol. 6, Dec. 1969, pp. 1404-1409.

[2] Martellucci, A. and Neff, R.S., "Influence of Asymmetric Transition on Re-Entry Vehicle Characteristics," *Journal of Spacecraft and Rockets*, Vol. 8, May 1971, pp. 476-482.

[3] Ericsson, L.E., "Transition Effects on Slender Vehicle Stability and Trim Characteristics," *Journal of Spacecraft and Rockets*, Vol. 11, Jan. 1974, pp. 3-11.

[4] Penland, J.A., "Aerodynamic Force Characteristics of a Series of Lifting Cone and Cone-Cylinder Configurations at a Mach Number of 6.83 and Angles of Attack Up to 130°," TN D-840, June 1961, NASA.

[5] Penland, J.A., "A Study of the Stability and Location of the Center of Pressure on Sharp, Right Circular Cones at Hypersonic Speeds," TN D-2283, May 1964, NASA.

[6] Truitt, R.W., *Hypersonic Aerodynamics*, Ronald Press, New York, 1959.

[7] Jones, D.J., "Numerical Solutions of the Flow Field for Conical Bodies in a Supersonic Stream," National Research Council of Canada, Ottawa, Aeronautical Rept. LR-507, July 1968.

[8] Jones, D.J., "Tables of Inviscid Supersonic Flow About Circular Cones at Incidence, $\gamma=1.4$, Parts I and II," AGARDograph 137, Nov. 1969.

[9] McGowan, J.J., III, and Davis, R.T., "Development of a Numerical Method to Solve the Three-Dimensional Compressible Laminar Boundary-Layer Equations with Application to Elliptical Cones at Angle of Attack," ARL 70-0341, Dec. 1970, Aerospace Research Labs., Wright-Patterson Air Force Base, Oh.

[10] Adams, J.C. Jr., "Three-Dimensional Laminar Boundary-Layer Analysis of Upwash Patterns and Entrained Vortex Formation on Sharp Cones at Angle of Attack," AEDC-TR-71-215 (AD736880), Dec. 1971, Arnold Engineering Development Center, Arnold Air Force Station, Tenn.

[11] Adams, J.C., Jr., "Analysis of the Three-Dimensional Compressible Turbulent Boundary Layer on a Sharp Cone at Incidence in Supersonic and Hypersonic Flow," AEDC-TR-72-66 (AD743003), June 1972, Arnold Engineering Development Center, Arnold Air Force Station, Tenn.

[12] Lubard, S.C. and Helliwell, W.S., "Calculation of the Flow on a Cone at High Angle of Attack," RDA-TR-150, Feb. 1973, R&D Associates, Santa Monica, Calif.; also *AIAA Journal*, Vol. 12, July 1974, pp. 965-974.

[13] Adams, J.C., Jr., "Numerical Calculation of the Three-Dimensional Hypersonic Viscous Shock Layer on a Sharp Cone at Incidence," Paper presented at the AIAA 2nd Computational Fluid Dynamics Conference, Hartford, Conn., June 1975.

[14] Garcia, F., Jr., "Comment on the Location of the Center of Pressure of a Right Circular Cone Using Newtonian Impact Theory," *AIAA Journal*, Vol. 4, June 1966, pp. 1150-1151.

[15] Lewis, C.H., Marchand, E.O., and Little, H.R., "Mass Transfer and First-Order Boundary-Layer Effects on Sharp Cone Drag, Part I: At Supersonic Conditions," *AIAA Journal*, Vol. 4, Oct. 1966, pp. 1697-1703.

[16] Lewis, CH., Marchand, E.O., and Little, H.R., "Mass Transfer and First-Order Boundary-Layer Effects on Sharp Cone Drag, Part II: At Hypersonic Conditions," *AIAA Journal*, Vol. 4, Nov. 1966, pp. 1954-1960.

[17] Horstman, C.C. and Kussoy, M.I., "Hypersonic Viscous Interaction on Slender Cones," *AIAA Journal*, Vol. 6, Dec. 1968, pp. 2364-2371.

[18] Feldhann, R.H., Winkelmann, A.E., and Pasiuk, L., "An Experimental Investigation of the Flow Field Around a Yawed Cone," *AIAA Journal*, Vol. 9, June 1971, pp. 1074-1081.

[19] Boericke, R.R., "Laminar Boundary Layer on a Cone at Incidence in Supersonic Flow," *AIAA Journal*, Vol. 9, Mar. 1971, pp. 462-468.

[20] Murdock, J.W., "The Solution of Sharp Cone Boundary Layer Equations in the Plane-of-Symmetry," *Journal of Fluid Mechanics*, Vol. 54, Pt. 4, Aug. 1972, pp. 665-678.

[21] Wu, P. and Libby, P.A., "Laminar Boundary Layer on a Cone Near a Plane of Symmetry," *AIAA Journal*, Vol. 11, Mar. 1973, pp. 326-333.